JOURNAL OF SPACECRAFT AND ROCKETS
Vol. 32, No. 3, May–June 1995

Fin Dihedral Effects on Wing-Body Carryover for Supersonic Noncircular Missiles

Brian E. Est* and H. F. Nelson†
University of Missouri—Rolla, Rolla, Missouri 65401

The aerodynamic effects of fin dihedral, Mach number, and fuselage cross section shape on wing-body carryover are investigated for supersonic, wing-body missiles at low angles of attack. A steady, three-dimensional, Euler code was used to numerically determine the normal force and center of pressure (CP) on infinitely thin delta wings in the presence of the missile body. The wing normal force is presented in terms of the component buildup parameter $K_{W(B)}$, a measure of the wing-body interference due to body upwash. $K_{W(B)}$ was found to be sensitive to dihedral, Mach number, and body cross-sectional shape. Fin dihedral influenced the wing CP for the inverted-triangular and triangular fuselage cross sections, but it did not appreciably affect the CP for circular, square, and diamond cross sections. For all fuselage cross sections, increasing Mach number moved the fin CP inboard. Changing the fuselage cross section from a circle to a diamond or triangle generally moved the fin CP outboard.

Nomenclature

a	= shape factor (Appendix)
$\mathcal{AR}$	= aspect ratio of wing formed by joining two fins
$C_{N_{W(B)}}$	= fin normal force coefficient in presence of body
$(C_{N_\alpha})_W$	= fin-alone normal force curve slope, deg^{-1}
$(C_{N_\alpha})_{W(B)}$	= fin normal force curve slope in presence of body, deg^{-1}
$K_{W(B)}$	= fin-body interference factor due to upwash
K_ϕ	= fin-fin interference factor due to sideslip
M_∞	= freestream Mach number
R	= radius of inscribed circle in fuselage base, cm
S	= fin semispan, measured from fuselage centerline, cm
y	= distance from the body centerline, cm
$\bar{y}$	= nondimensional distance from the body centerline, y/R
Z	= axial distance from missile nosetip, cm
Z_{LE}	= axial distance to fin root chord leading edge, cm
$\bar{z}$	= axial distance behind leading edge of fin, $(Z - Z_{LE})/R$
α	= missile angle of attack, deg
α_{eq}	= fin equivalent angle of attack, deg
β	= missile sideslip angle, deg
Γ	= fin dihedral angle, deg
$(\Delta\alpha)_v$	= induced change in α due to vorticies
Λ	= fin leading-edge sweepback angle, 51.34 deg

Introduction

THE cross-sectional shape of missile launch tubes is triangular for airborne rotary launchers and square for armored box launchers. Missiles with square or triangular fuselage cross sections optimize launcher cross-sectional area and have shown the potential for increased maneuverability and larger lift/drag ratios than missiles with circular fuselage cross sections.[1–6]

A variety of missile configurations and component arrangements are studied during conceptual and preliminary missile design; consequently, the missile designer needs inexpensive, fast methods that accurately predict missile lift and center of pressure, because of time and cost constraints. Component buildup methods have received much attention in missile literature.[7–9] Correlations of analytical or experimental data can easily be incorporated into the component buildup analysis to yield fast and accurate predictions. The total missile normal force is determined by adding the individual component contributions while using carryover factors to account for their mutual interference. In some instances the fin-body carryover contribution to missile normal force can be larger than the fin-alone contribution.

The equivalent angle-of-attack component buildup method[10–13] evaluates body upwash, sideslip, and vortex effects to compute an equivalent angle of attack for the fin on the missile. For a missile fin at low angle of attack the normal force is

$$C_{N_{W(B)}} = \alpha_{eq}\left(C_{N_\alpha}\right)_W \tag{1}$$

where the fin equivalent angle of attack is

$$\alpha_{eq} = K_{W(B)}\alpha + (4/\mathcal{AR})K_\phi\alpha\beta + (\Delta\alpha)_v \tag{2}$$

$K_{W(B)}$, K_ϕ, $(\Delta\alpha)_v$, and $(C_{N_\alpha})_W$ represent the interference contribution due to body upwash, fin-fin interaction due to sideslip, vortex effects, and the wing-alone normal force curve slope, respectively. The body upwash component is defined as

$$K_{W(B)} = \frac{\left(C_{N_\alpha}\right)_{W(B)}}{\left(C_{N_\alpha}\right)_W} \tag{3}$$

The objective of this investigation is to explore the effects of fin dihedral, Mach number, and fuselage cross section shape on $K_{W(B)}$ and fin center of pressure (CP) for body-tail, cruciform missiles in supersonic cruise for use in conceptual and preliminary design. Fuselages with circular, square, diamond, triangular, and inverted-triangular cross sections are considered.

Analytical Methodology

Governing Equations

The inviscid shock layer for tactical missiles in supersonic flight can be predicted by numerically solving the three-dimensional, steady Euler equations.[1,14–18] The zonal Euler solver (ZEUS),[17–20] a finite-volume, space-marching Euler code, was used in this investigation because of its robustness, computational efficiency, and second-order accuracy. The flowfield between the missile body and

Presented as Paper 91-3256 at the AIAA 9th Applied Aerodynamic Conference, Baltimore, MD, Sept. 23–25, 1991; received Oct. 4, 1991; revision received March 23, 1993; accepted for publication April 12, 1993.

*Graduate Student, Department of Mechanical and Aerospace Engineering and Engineering Mechanics; currently Aerospace Engineer, Flight Vehicle Analysis Branch, Dynetics, Inc., Huntsville, AL 35814. Member AIAA.

†Professor of Aerospace Engineering, Thermal Radiative Transfer Group, Department of Mechanical and Aerospace Engineering and Engineering Mechanics. Associate Fellow AIAA.

the bow shock was generated with the bow shock treated as a discontinuity. ZEUS is also capable of capturing the bow shock. The predicted pressure distribution was integrated over the missile surface to obtain force and moment data.

At α greater than about 4 deg, the viscous flow about missile bodies with circular cross sections tends to separate and roll up to form leeside vortices. The strength of these vortices becomes significant at large angles of attack. For missiles with noncircular fuselage cross sections, viscous effects may become important at lower α. Corners of square and triangular fuselages cause boundary layer separation resulting in shed vortices, which produces nonlinear angle-of-attack effects on missile lift. The Euler equations do not predict viscous vortex shedding, but work exists that shows that it is not substantial for $\alpha < 5$ deg. Jorgensen[5] performed a wind tunnel test with flow visualization for forebodies with square and triangular cross-sectional shapes with shape parameters a of 0.9748 and 0.9834 (see Appendix), respectively at $M_\infty = 1.98$ and 3.88 for α from 0 to 17 deg. For $\alpha > 5$ deg the corners produced strong leeside vortex systems.

ZEUS has been shown to predict accurate forces and moments on missiles.[15–20] Est and Nelson[21] compared ZEUS predictions of lift with wind tunnel data at $M_\infty = 2.01$ for forebodies with square and triangular cross sections with $a = 0.5122$ and 0.5580, respectively. Their results showed good agreement for lift coefficient for $\alpha \leq 6$ deg. The fuselage cross sections examined in the present research have shape parameters ranging from 0 to 0.5 and the calculations are at $\alpha = 3$ deg; therefore, viscous effects should be small and the Euler equations should accurately model the flowfield.

Body Cross-Sectional Shape and Fin Position

All of the body cross-sectional shapes investigated are related by a shape parameter a, which is derived and illustrated in the Appendix. As a varies from 0 to 1 it quantifies the fuselage cross-sectional shape. When $a = 0$, all shapes are circular with a common radius R. When $a = 1$, the shapes are sharp-cornered squares or triangles, depending upon the shape of interest.

The reference positions ($\Gamma = 0$ deg) of the fins for the fuselage cross sections of the present research are shown in Fig. 1. For the circle, square, and diamond fuselage cross sections, the fins are arranged equidistant in a "plus" configuration. For the triangular and inverted triangular fuselages, the fins are arranged in a "plus" configuration, but are not equidistant. The horizontal fins are located in the horizontal plane that passes through the shoulders of the equilateral triangles. The fin reference positions were governed by the requirement that the fins be folded when the missile is in the launch tube.

The fin root chord is located at $y/R = 1$ for the circle and square cross sections; however, for the triangle, diamond, and inverted

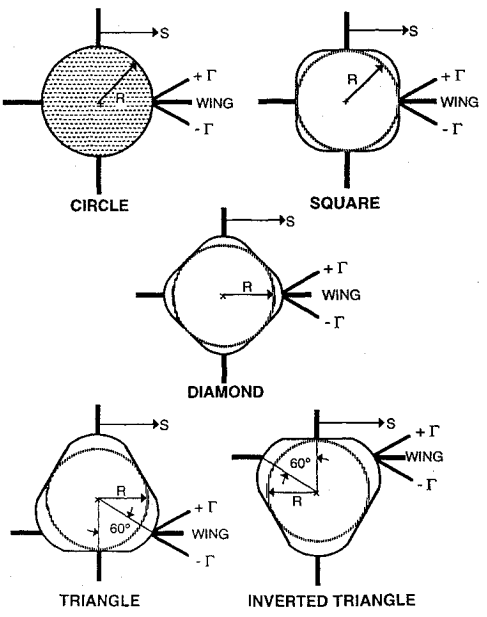

Fig. 1 Fuselage cross-sectional shapes and baseline fin positions.

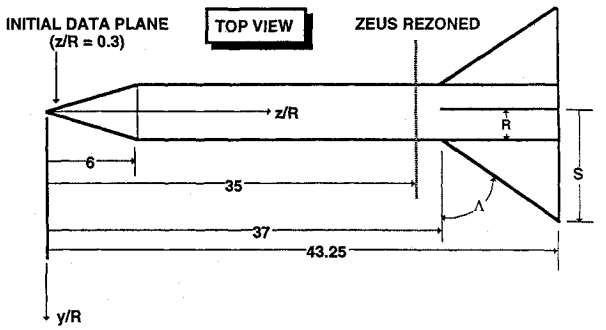

Fig. 2 Missile geometry.

triangle the fin root chord is at $y/R \geq 1$, e.g., at $y/R = 1.299$ for a fin on an $a = 0.5$ triangle fuselage (see Fig. 1). The fin root chord y/R position is a function of shape parameter, a. When the shape of the fuselage is changed (changing a) the position of the fin root chord shifts relative to the fuselage centerline, resulting in shifted values of S/R. For data comparison purposes, it was not practical to account for this shift. Therefore, the position $S/R = 1$ is always located at the fin root chord independent of the body cross section and the position $S/R = 6$ implies a fin with a span that extends outward five body radii ($5R$) from the fin root chord.

$K_{W(B)}$ is defined as the missile fin normal force curve slope divided by the fin-alone normal force curve slope in Eq. (3). For the baseline case $\Gamma = 0$ deg, all of the wing normal force is contained in the $K_{W(B)}$ term; however, for wings with dihedral the force on the fin breaks into yaw and normal components. The fin normal component is used in the $K_{W(B)}$ evaluation. For unbanked missiles with pitch plane symmetry, no net yawing force develops due to wing dihedral.

Missile Configuration

Figure 2 presents the missile geometry used in this research. The nose cone of the missile is conical for $Z/R \leq 0.3$. For $0.3 < Z/R < 6$ the cross section changes linearly with Z/R from a circle to the cross-sectional shape of interest. For $Z/R \geq 6$, the cross section is constant. The computations begin at an initial data plane that is generated by a one-dimensional conical starting solution that takes the calculations across the bow shock at the tip of the missile to $Z/R = 0.3$. The computational grid used in this research was developed in a mesh refinement study. It was configured as a single zone with a 36×36 (r by ϕ) mesh for the forebody calculations in the range $0.3 \leq Z/R \leq 35$ and run at 90% the Courant–Friedrichs–Lewy (CFL) stability condition step limit. At $Z/R = 35$, the code was rezoned and restarted with two, (36×36) zones for $35 \leq Z/R \leq 43.25$ and run at 20% of the CFL limit to more accurately calculate the flow over the missile fins. Reducing the maximum CFL limit reduced the computational marching step, in effect, increasing the number of grid points on the fins. Pitch plane symmetry was utilized to reduce computer storage and run time. For simplicity mesh clustering was not used. All of the computations were made using the IBM 4381 computer at the University of Missouri—Rolla. CPU times up to 2 h were required for complete flowfield solutions over the entire missile.

Wing-Alone Lift

The fins used in this research were infinitely thin delta wings in a "plus" configuration. Supersonic lifting surface theory was used to determine the wing-alone normal force curve slope, which is

$$(C_{N_\alpha})_W = \frac{4\cos\Gamma}{\sqrt{M_\infty^2 - 1}} \tag{4}$$

for supersonic leading edges. At low angles of attack, supersonic lifting surface theory yields accurate predictions of $(C_{N_\alpha})_W$ for delta fins. All the data presented herein are normalized by $(C_{N_\alpha})_W$ at $\Gamma = 0$ deg.

Small S/R Considerations

For $S/R < 2$, the prediction of $C_{N_{W(B)}}$ becomes inaccurate due to the small number of grid points located on the fin. Experimen-

Table 1 $K_{W(B)}$ values from potential flow at $S/R = 1$

Cross-sectional shape	Shape factor				
	$a = 0.0$	$a = 0.25$[a]	$a = 0.50$[a]	$a = 0.60$	$a = 0.65$
Square	2.00	1.77	1.53	1.50	—
Diamond	2.00	2.05	2.10	2.12	—
Triangle	1.50	1.59	1.68	—	1.73
Inv. triangle	1.50	1.59	1.68	—	1.73

[a]Denotes linearly interpolated data.

tal data and potential flow solutions exist for surface pressure for flow over cylinders with noncircular cross sections.[22] In the limit as S/R approaches one, the current numerical calculations should approach these potential flow solutions. Thus, the $K_{W(B)}$ values can be extrapolated from $S/R = 2$ to match the potential flow solutions at $S/R = 1$. Reference 22 presents surface pressure data for circular shapes ($a = 0$) and for square and triangular shapes with $a = 0.6$ and 0.65, respectively. These data were linearly interpolated in a to find $K_{W(B)}$ at $S/R = 1$ for the shape factors of interest. Table 1 presents the potential flow values of $K_{W(B)}$ in the limit as S/R goes to 1. The value of $K_{W(B)}$ for circular shapes ($a = 0$) at $S/R = 1$ is 2 when the fin is on the centerline; however, when the fin is displaced either up or down from the centerline (as it is for the triangle and inverted triangle, see Fig. 1) $K_{W(B)}$ decreases.

Results and Discussion

The nominal flight conditions were $M_\infty = 3, \alpha = 3$ deg, and $\Lambda = 51.34$ deg. $K_{W(B)}$ and fin CP data are presented for $2 \leq M_\infty \leq 4, 0 \leq a \leq 0.5$, and $-10 \leq \Gamma \leq 10$ deg. The fins are planar, delta fins with zero thickness. The leading edge of the fin root chord was located at $Z/R = 37$ and root chord length was increased to increase S/R. The root chord leading edge was located $31R$ behind the nose cone–body junction to minimize nose cone effects. The transition from a circular cross section to the final cross section along the nose cone effects the bow shock shape and hence the entropy distribution near the missile surface in the fin region. These vortical effects are probably negligible at Mach 2, but may be important at Mach 4. These effects were not considered in the present analysis.

Fin Dihedral Effects

The effect of fin dihedral on the flowfield is illustrated by crossflow velocity vectors in Figs. 3 and 4. Dihedral alters the shock and expansion waves near the fuselage. Figure 3 shows the velocity field near a triangular fuselage with a fin at $\Gamma = -10$ deg. It shows the windward shock and the leeward expansion due to the fin. Figure 4 shows the velocity field near an inverted triangle fuselage with a fin at $\Gamma = 5$ deg. The flowfield above the fin is very complicated and it even contains a reverse-flow region at the top of the body. The windward shock below the fin is well defined.

The circle symbols on Figs. 5–10 show slender-body theory (SBT) results from Ref. 11 for a missile with a circular body with its fins on the centerline at $\Gamma = 0$ deg. SBT results are a function of S/R only and are shown to indicate that the ZEUS results are of similar magnitude.

Figure 5 shows the effect of Γ on $K_{W(B)}$ for inverted-triangular fuselages as a function of S/R. As Γ increases from -10 to 10 deg, $K_{W(B)}$ decreases for all S/R. This occurs because of changes in the pressure in the region between the fuselage and the underside of the fin. For negative dihedral the fin tends to trap the crossflow, which increases the pressure under the fin. As Γ increases from negative to positive angles the pressure under the fin decreases. When the fin dihedral angle becomes positive the crossflow velocity under the fin is channeled outboard, reducing pressure. On the upper surface of the fin the expansion processes do not change very much as Γ increases from -10 to 10 deg. These effects combine to reduce the pressure difference between the fin's top and bottom surfaces; consequently, the normal force on the fin and $K_{W(B)}$ decrease as Γ increases.

Figure 6 shows $K_{W(B)}$ vs S/R for $-10 \leq \Gamma \leq 10$ deg for missiles with square fuselages. Negative values of Γ have little effect on $K_{W(B)}$; however, increasing Γ from 0 to 10 deg reduces $K_{W(B)}$ at all S/R. The corners on the square fuselage tend to reduce the spread in $K_{W(B)}$ data and increase the rate of decrease of $K_{W(B)}$ with S/R at small S/R compared to the inverted triangle fuselage for $-10 \leq \Gamma \leq 10$ deg.

Body Cross-Sectional Shape Effects

Figure 7 presents the effect of changing the cross section from a circle to a square (increasing a) on $K_{W(B)}$ for a range of S/R at $\Gamma = -10$ deg. As a increases, $K_{W(B)}$ decreases for $S/R \leq 6$. Body shape does not influence the flowfield very much for $S/R > 5$, because for large fin spans most of the fin normal force is produced beyond the influence of the body. The $a = 0$ (circle fuselage) data agree reasonably well with SBT, even though $\Gamma = -10$ deg. The reduction in $K_{W(B)}$ with S/R at small S/R is due to the change in pressure as the crossflow expands around the windward corner of the square body. The flat bottom of the square cross section acts to maintain the surface pressure close to the crossflow stagnation pressure along

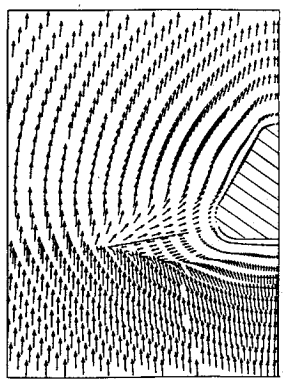

Fig. 3 Crossflow velocity vectors for a triangular fuselage cross section with $\Gamma = -10$ deg, $S/R = 4$, $M_\infty = 4$, $a = 0.5$, and $\alpha = 3$ deg.

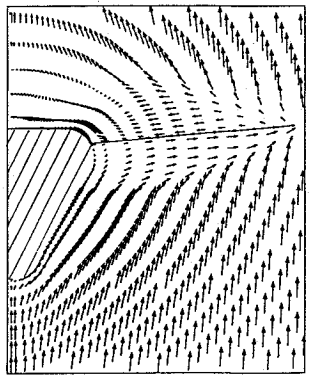

Fig. 4 Crossflow velocity vectors for an inverted-triangular fuselage cross section with $S/R = 5$, $\Gamma = 5$ deg, $M_\infty = 4$, $a = 0.5$, and $\alpha = 3$ deg.

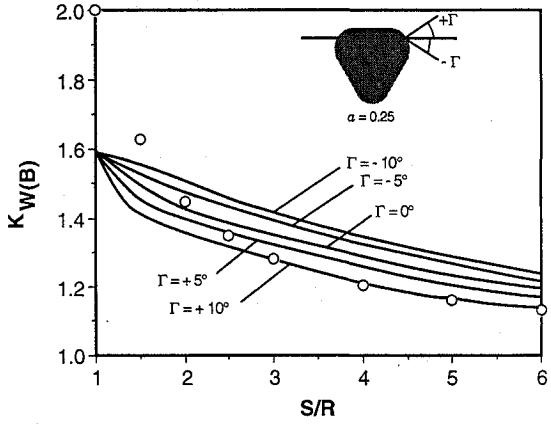

Fig. 5 $K_{W(B)}$ vs S/R for several values of Γ for missiles with inverted triangular cross sections at $M_\infty = 3$, $\alpha = 3$ deg, $a = 0.25$; the ○ are SBT results for a circular body at $\Gamma = 0$.

the bottom of the fuselage. The pressure near the body decreases during the expansion as the crossflow turns the windward corner, ultimately reducing the normal force on the fin. As a increases the corner becomes sharper and the expansion becomes greater, which further reduces the fin lift.

Figure 8 presents the effect of changing the cross section from a circle to an inverted triangle (increasing a) on $K_{W(B)}$ for a range of S/R at $\Gamma = -10$ deg. As the cross section becomes more triangular, $K_{W(B)}$ increases. This trend is the opposite of that of the square. The body and fin act to increase the compression below the fin and the expansion above the fin as a increases, because the shape changes from a circle to an inverted triangle. This results in larger $K_{W(B)}$ values. Note that the $a = 0$ case of Figs. 7 and 8 is different due to different fin vertical positions on the missile fuselage. Also, the curves on Figs. 7 and 8 for each shape factor approach the same limit as S/R becomes large, because the fin lift becomes independent of the fuselage shape. For the inverted triangle of Fig. 8 this occurs at S/R greater than 6.

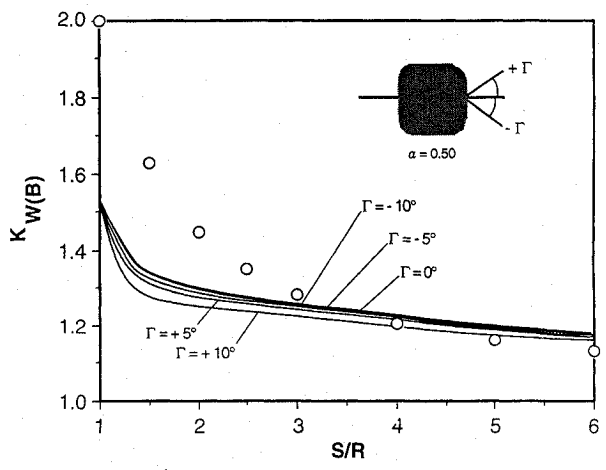

Fig. 6 $K_{W(B)}$ **vs** S/R **for several values of** Γ **for a missile with square cross section at** $M_\infty = 3$, $\alpha = 3$ **deg,** $a = 0.5$; **the** o **are SBT results for a circular body at** $\Gamma = 0$ **deg.**

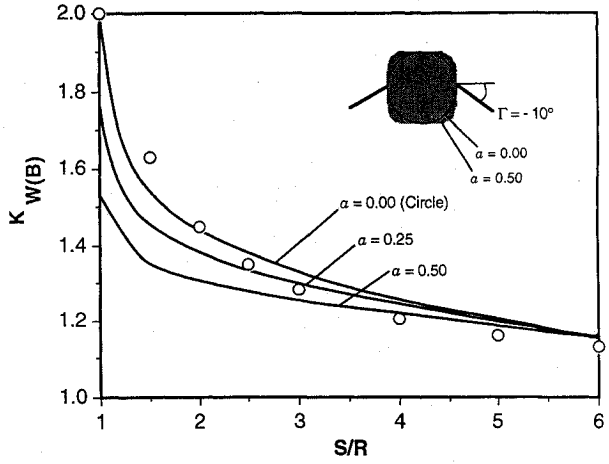

Fig. 7 Shape factor effects on $K_{W(B)}$ **for missiles with square fuselage cross sections as a function of** S/R **at** $M_\infty = 3$, $\alpha = 3$ **deg,** $\Gamma = -10$ **deg; the** o **are SBT results for a circular body at** $\Gamma = 0$ **deg.**

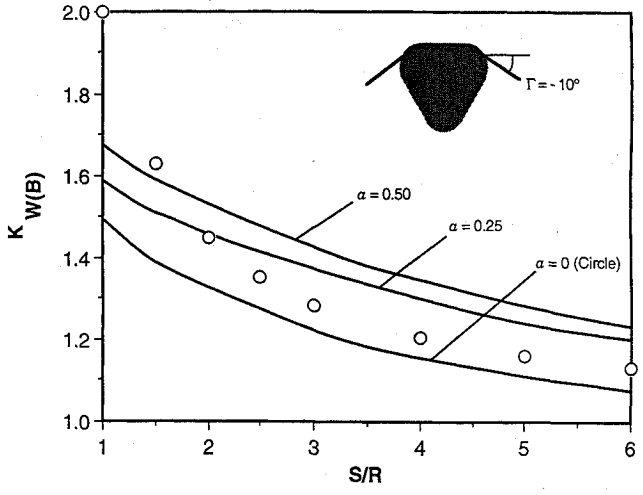

Fig. 8 Shape factor effects on $K_{W(B)}$ **for inverted-triangular fuselage cross sections at** $M_\infty = 3$, $\alpha = 3$ **deg,** $\Gamma = -10$ **deg; the** o **are SBT results for a circular body at** $\Gamma = 0$ **deg.**

Mach Number Effects

Figures 9 and 10 show $K_{W(B)}$ vs S/R for 3 Mach numbers at $\Gamma = -10$ deg for square and triangular fuselage cross sections, respectively. Increasing M_∞ increases $K_{W(B)}$ for both fuselage shapes at all S/R. As M_∞ increases, the pressure on the bottom surface of the fin behind the windward shock increases and the pressure on the top surface of the fin behind the expansion decreases. This yields larger pressure differences between the bottom and top fin surface, hence a larger $K_{W(B)}$.

Fin Center of Pressure

The CP position is influenced by M_∞, Γ, S/R, and a. Figure 11 shows the effect of a on fin CP as a function of S/R for inverted-triangular fuselages for $\Gamma = 10$ deg. $\bar{z}_{CP} = 0$ corresponds to the fin root chord leading edge on the z-axis. At $\bar{z}_{CP} = 0$, $\bar{y}_{CP}$ increases as

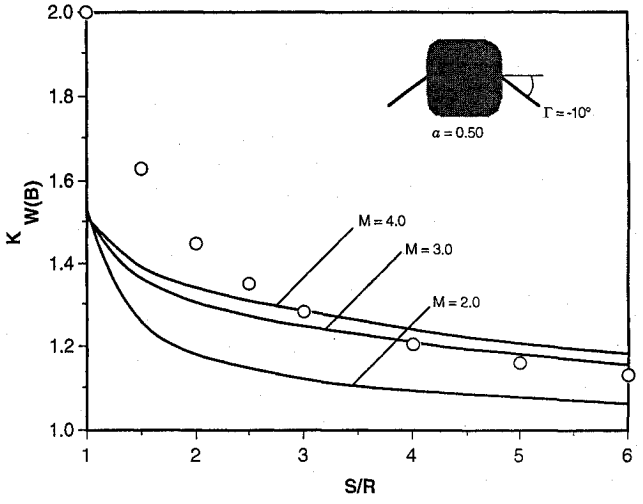

Fig. 9 Mach number effects on $K_{W(B)}$ **for square fuselage cross sections at** $\Gamma = -10$ **deg,** $\alpha = 3$ **deg,** $a = 0.5$; **the** o **are SBT results for a circular body at** $\Gamma = 0$ **deg.**

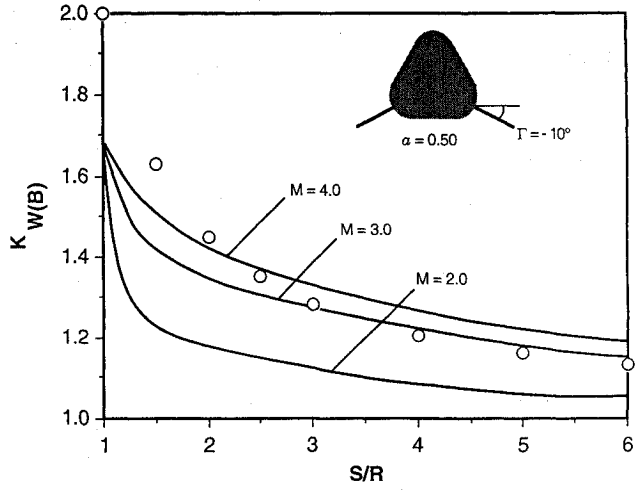

Fig. 10 Mach number effects on $K_{W(B)}$ **for triangular cross sections at** $\Gamma = -10$ **deg,** $\alpha = 3$ **deg,** $a = 0.5$; **the** o **are SBT results for a circular body at** $\Gamma = 0$ **deg.**

Table 2 Parametric effects on $K_{W(B)}$ and CP

	$K_{W(B)}$				
	Fuselage cross-sectional shape				
Parameter	Triangle	Inv. triangle	Square	Circle	Diamond
Decreasing Γ					
0 to −10 deg	none	higher	none	none	none
Increasing Γ					
0 to 10 deg	higher	lower	lower	none	none
Increasing M_∞	higher	higher	higher	higher	higher
Increasing a	lower	higher	lower	—	none
	Fin CP location				
	Fuselage cross-sectional shape				
Parameter	Triangle	Inv. triangle	Square	Circle	Diamond
Decreasing Γ		move			
0 to −10 deg	none	outboard	none	none	none
Increasing Γ	move				
0 to 10 deg	outboard	none	none	none	none
Increasing M_∞	move	move	move	move	move
	inboard	inboard	inboard	inboard	inboard
Increasing a	move	move		—	move
	outboard	outboard	none	—	outboard

Table 3 $K_{W(B)}$ for circle and square cross sections

	$K_{W(B)}$		S/R							
M	a	Γ deg	1	1.5	2	2.5	3	4	5	6
3	0	10	2.00	1.536	1.452	1.389	1.338	1.261	1.207	1.166
	0	0	2.00	1.530	1.450	1.387	1.337	1.262	1.209	1.169
	0	−10	2.00	1.529	1.447	1.380	1.328	1.250	1.193	1.151
3	0.5	10	1.53	1.270	1.253	1.240	1.226	1.198	1.169	1.141
	0.5	0	1.53	1.322	1.300	1.283	1.265	1.233	1.203	1.174
	0.5	−10	1.53	1.344	1.315	1.289	1.265	1.226	1.191	1.158
2	0.5	10	1.53	1.219	1.167	1.152	1.141	1.111	1.080	1.052
	0.5	0	1.53	1.253	1.191	1.174	1.165	1.136	1.106	1.079
	0.5	−10	1.53	1.245	1.182	1.164	1.151	1.120	1.088	1.060
4	0.5	10	1.53	1.273	1.265	1.252	1.238	1.209	1.184	1.162
	0.5	0	1.53	1.331	1.323	1.308	1.289	1.254	1.225	1.200
	0.5	−10	1.53	1.350	1.342	1.320	1.297	1.252	1.217	1.187

Table 4 $K_{W(B)}$ for triangular cross sections

	$K_{W(B)}$		S/R							
M	a	Γ deg	1	1.5	2	2.5	3	4	5	6
3	0.5	10	1.68	1.308	1.365	1.381	1.368	1.316	1.263	1.220
	0.5	0	1.68	1.190	1.271	1.294	1.291	1.260	1.221	1.188
	0.5	−10	1.68	1.298	1.307	1.302	1.283	1.234	1.188	1.152
2	0.5	10	1.68	1.194	1.185	1.202	1.204	1.185	1.157	1.132
	0.5	0	1.68	1.022	1.055	1.078	1.082	1.093	1.081	1.069
	0.5	−10	1.68	1.147	1.097	1.097	1.097	1.091	1.077	1.062
4	0.5	10	1.68	1.348	1.419	1.427	1.409	1.354	1.300	1.257
	0.5	0	1.68	1.271	1.362	1.377	1.367	1.323	1.278	1.239
	0.5	−10	1.68	1.396	1.404	1.383	1.352	1.290	1.238	1.197

Table 5 $K_{W(B)}$ for inverted-triangular cross sections

	$K_{W(B)}$		S/R							
M	a	Γ deg	1	1.5	2	2.5	3	4	5	6
3	0.5	10	1.68	1.398	1.366	1.334	1.297	1.231	1.180	1.145
	0.5	0	1.68	1.350	1.407	1.395	1.364	1.302	1.245	1.207
	0.5	−10	1.68	1.494	1.515	1.489	1.448	1.366	1.297	1.246
2	0.5	10	1.68	1.277	1.206	1.175	1.148	1.117	1.091	1.069
	0.5	0	1.68	1.188	1.211	1.206	1.186	1.165	1.135	1.114
	0.5	−10	1.68	1.385	1.352	1.330	1.298	1.244	1.199	1.163
4	0.5	10	1.68	1.382	1.361	1.336	1.309	1.255	1.212	1.175
	0.5	0	1.68	1.368	1.420	1.415	1.395	1.339	1.289	1.247
	0.5	−10	1.68	1.479	1.513	1.499	1.469	1.398	1.335	1.284

Table 6 $K_{W(B)}$ for diamond cross sections

$K_{W(B)}$			S/R							
M	a	Γ deg	1	1.5	2	2.5	3	4	5	6
3	0.5	10	2.10	1.530	1.458	1.393	1.339	1.257	1.199	1.074
	0.5	0	2.10	1.561	1.488	1.426	1.373	1.291	1.231	1.103
	0.5	−10	2.10	1.542	1.478	1.415	1.361	1.276	1.214	1.091
2	0.5	10	2.10	1.321	1.244	1.207	1.177	1.124	1.086	0.978
	0.5	0	2.10	1.346	1.268	1.230	1.201	1.151	1.114	1.003
	0.5	−10	2.10	1.322	1.252	1.216	1.188	1.135	1.097	0.986
4	0.5	10	2.10	1.626	1.529	1.449	1.389	1.297	1.234	1.101
	0.5	0	2.10	1.670	1.575	1.495	1.430	1.338	1.273	1.139
	0.5	−10	2.10	1.666	1.575	1.492	1.424	1.326	1.258	1.123

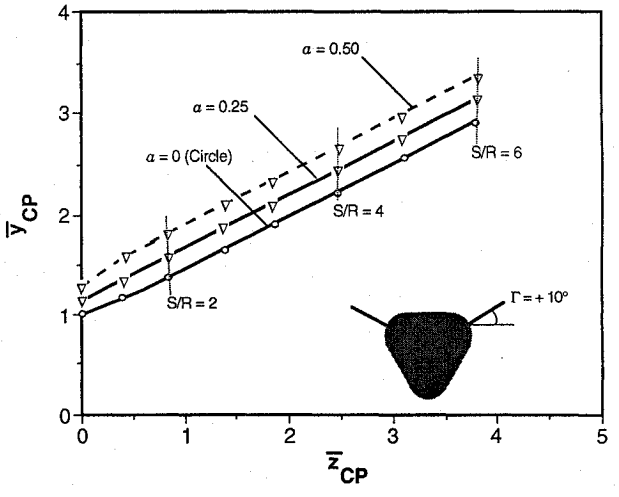

Fig. 11 Effect of changing a and S/R on fin CP for inverted-triangular cross sections at $\Gamma = 10$ deg, $M_\infty = 3$, $\alpha = 3$ deg; the symbols are at $S/R = 1$, 1.5, 2, 2.5, 3, 4, 5, and 6.

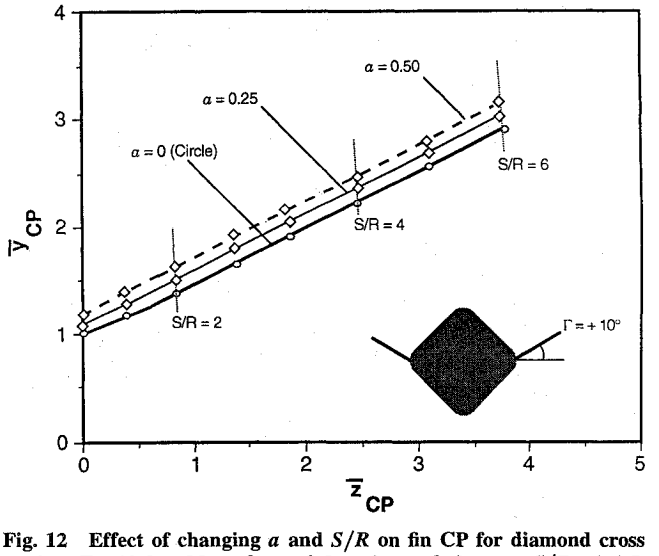

Fig. 12 Effect of changing a and S/R on fin CP for diamond cross sections $\Gamma = 10$ deg, $M_\infty = 3$, $\alpha = 3$ deg; the symbols are at $S/R = 1$, 1.5, 2, 2.5, 3, 4, 5, and 6.

a increases because $\bar{y}_{CP}$ is measured from the fuselage centerline. In other words, the fuselage becomes wider as a increases. Recall that $\bar{y}_{CP}$ is not corrected for the varying fin root chord locations for the triangular, inverted-triangular and diamond fuselages ($\bar{y}_{CP} = 0$ is the body centerline). Figure 12 shows the effect of increasing a on fin CP position as a function of S/R for diamond fuselages with $\Gamma = 10$ deg. The fin CP is translated outboard with increasing a because the body corner moves outward as a increases. In both Figs. 11 and 12, the CP is generally located at the geometric centroid of the fin planform and moves outboard as a increases at a specific

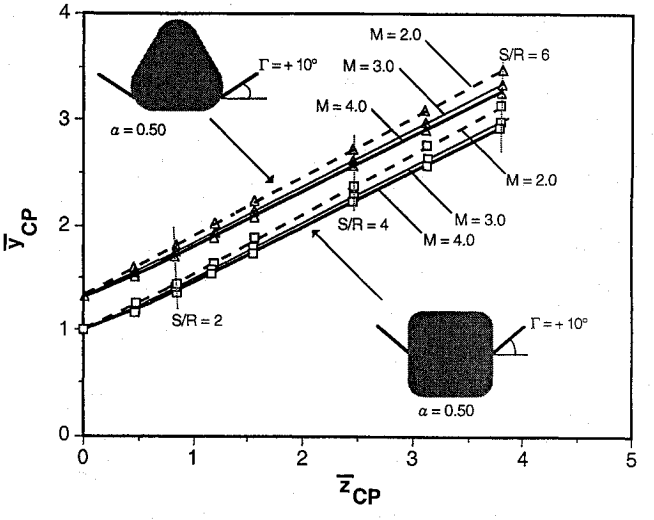

Fig. 13 Effect of changing M_∞ and S/R on fin CP for square and triangular fuselage cross sections at $\Gamma = 10$ deg, $a = 0.5$, $\alpha = 3$ deg; the symbols are at $S/R = 1$, 1.5, 2, 2.5, 3, 4, 5, and 6.

value of S/R. The slopes of the lines with different a values are essentially identical. The movement of the CP in the z direction is due to the increase in the root chord as S/R increases.

The effect of M_∞ and S/R on CP location is shown in Fig. 13 for square and triangular fuselages for $\Gamma = 10$ deg. The CP moves inboard at a specific value of S/R as M_∞ increases, but it is still generally located near the fin geometric centroid. As M_∞ increases, the inboard area of the fin experiences a larger increase in normal force than the outboard area (see Figs. 9 and 10), which moves CP inboard.

Tabulated Results

All of the $K_{W(B)}$ and CP data are tabulated in Refs. 1 and 24 as a function of M_∞, α, Γ, and S/R for use in conceptual and preliminary design. Tables 3–6 give $K_{W(B)}$ data as a function of S/R for each cross section at $M_\infty = 3$ and $\alpha = 3$ deg. The data can be used for comparison to analytical or experimental results. Also, the tabulated $K_{W(B)}$ and CP values can be used as table lookup data, or can be curve fit and incorporated into an existing aeroprediction program.

Conclusions

An Euler code has been used to determine $K_{W(B)}$ and fin CP for cruciform missiles in supersonic cruise. Fin dihedral was varied from −10 to 10 deg for missiles with circular, square, diamond, triangular and inverted-triangular fuselage cross sections. The fins were zero-thickness, planar delta fins and their spans varied from $S/R = 1$ to 6. $K_{W(B)}$ and fin CP are sensitive to fin dihedral angle, Mach number, fin span, and fuselage cross-sectional shape. Table 2 summarizes the effects of changing Γ, M_∞, S/R and a on $K_{W(B)}$ and CP. The data for circular fuselages are from Ref. 23.

It is shown that $K_{W(B)}$ decreases as S/R increases for missiles with noncircular fuselage cross sections. $K_{W(B)} > 1$ throughout the S/R range for all the fuselage shapes. This indicates that the fin

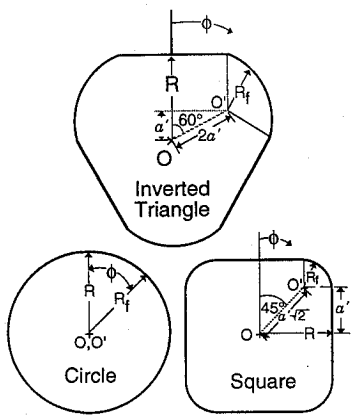

Fig. A1 Shape factor geometry.

produces greater normal force in the presence of the fuselage than when it is isolated (favorable interference).

The effect of changing the fuselage cross section from circular to square or triangular shape decreases $K_{W(B)}$, while changing from a circle to an inverted triangle increases $K_{W(B)}$, at any value of Γ. Body cross-sectional shape changes from a circle to a diamond have little effect on $K_{W(B)}$. CP tends to move outward as the fuselage is changed from a circle to a diamond or triangle shape. Changing from a circle to a square has little effect on CP. Also, Γ has little effect on CP.

Increasing M_∞ generally increases $K_{W(B)}$ and moves CP inboard for all fuselage shapes and fin spans. This trend is important in missile stability and control for accelerating flight.

Appendix: Development of the Shape Factor Parameter *a*

Parameter a quantifies the cross sectional shape of the missile fuselage. At $a = 0$, the shape is circular and at $a = 1$, the shape is the sharp-cornered shape of interest, i.e., a sharp-cornered square. Figure A1 shows the relationship between the shape factor and geometry of the noncircular fuselage cross sections. For the square cross sections, the circular fillet, defined by R_f, is enscribed over an arc of 90 deg. For the triangular cross sections, R_f is enscribed over 120 deg. For the circular cross section, the fillet enscribes a circle.

R_f and a' are defined in terms of the radius R of the inscribed circle (Fig. A1)

$$R = R_f + a' \tag{A1}$$

Thus one can write

$$a'/R + R_f/R = 1 \tag{A2}$$

However, the parameter a is defined as a'/R so that

$$a = 1 - R_f/R \tag{A3}$$

As a approaches 0, R_f approaches R, and as a approaches, 1 R_f approaches 0. For all shapes in this research R was 1 cm so that all fuselage shapes collapse to an identical, circular cross section at $a = 0$.

Acknowledgments

This work has been supported by McDonnell Douglas Missile Systems Company of St. Louis, Missouri, through the Independent Research and Development Program, monitored by Kurt D. Bausch. Additional funds were provided by the Missouri Research Assistance Act.

References

[1]Est, B. E., "Computational Aerodynamics of Supersonic Missiles with Noncircular Fuselage Cross Section," M.S. Thesis, Dept. of Mechanical and Aerospace Engineering, Univ. of Missouri–Rolla, MO, May 1991.

[2]Sigal, A., and Lapidot, E., "Aerodynamic Characteristics of Configurations Having Bodies with Square, Rectangular, and Circular Cross-Sections," *Journal of Spacecraft and Rockets*, Vol. 26, No. 2, 1989, pp. 85–89.

[3]Hutt, G. R., and Howe, A. J., "Effects of Cross Section and Nose Geometry on Slender-Body Supersonic Aerodynamics," *Journal of Spacecraft and Rockets*, Vol. 25, No. 2, 1988, pp. 189–193.

[4]Carlson, H. W., and Gapcynski, J. P., "An Experimental Investigation at a Mach Number of 2.01 of the Effects of Body Cross-Section Shape on the Aerodynamic Characteristics of Bodies and Wing-Body Combinations," NACA RM L55E23, July 1955.

[5]Jorgensen, L. H., "Inclined Bodies of Various Cross Sections at Supersonic Speeds," NASA Memo 10-3-58A, Nov. 1958.

[6]Sigal, A., "Analysis Methods and Experiments for Missiles with Noncircular Fuselages," *Tactical Missile Aerodynamics: Prediction Methodology*, edited by M. R. Mendenhall, Vol. 142, Progress in Aeronautics and Astronautics, AIAA, Washington, DC, 1991, pp. 171–213.

[7]Vukelich, S. R., and Jenkins, J. E., "Evaluation of Component Buildup Methods for Missile Aerodynamic Predictions," *Journal of Spacecraft and Rockets*, Vol. 19, No. 6, 1982, pp. 481–488.

[8]Stoy, S. L., and Vukelich, S. R., "Prediction of Aerodynamic Characteristics of Unconventional Missile Configurations Using Component Buildup Technique," AIAA Paper 86-0489, Jan. 1986.

[9]Hemsch, M. J., "Component Build-Up Method for Engineering Analysis of Missiles at Low-to-High Angles of Attack," *Tactical Missile Aerodynamics: Prediction Methodology*, Edited by M. R. Mendenhall, Vol. 142, Progress in Aeronautics and Astronautics, AIAA, Washington DC, 1991, pp. 115–169.

[10]Pitts, W. C., Nielsen, J. N., and Kaatari, G. E., "Lift and Center of Pressure of Wing-Body-Tail Combinations at Subsonic, Transonic, and Supersonic Speeds," NACA Rept. 1307, July 1953.

[11]Nielsen, J. N., *Missile Aerodynamics*, McGraw–Hill, New York, 1960; republished by Nielsen Engineering and Research, Mountain View, CA, 1988, Chap. 5.

[12]Stoy, S. L., and Vukelich, S. R., "Extension of the Equivalent Angle of Attack Prediction Method," AIAA Paper 84-0311, Jan. 1984.

[13]Hemsch, M. J., and Nielsen, J. N., "Extension of Equivalent Angle of Attack Method for Nonlinear Flowfields," *Journal of Spacecraft and Rockets*, Vol. 22, No. 3, 1985, pp. 304–308.

[14]Lijewski, L. E., "Transonic Euler Solutions on a Blunt, Body-Wing-Canard Configuration," *Journal of Spacecraft and Rockets*, Vol. 25, No. 6, 1988, pp. 393–399.

[15]Priolo, F. J., and Wardlaw, A. B., "Supersonic Non-Circular Missile Computations," *Journal of Spacecraft and Rockets*, Vol. 26, No. 3, 1989, pp. 151–157.

[16]Nelson, H. F., "Wing-Body Interference Lift for Supersonic Missiles with Elliptic Cross-Section Fuselages," *Journal of Spacecraft and Rockets*, Vol. 26, No. 5, 1989, pp. 322–329.

[17]Hall, D. W., Hines, R. W., Baltakis, F. P., and Wardlaw, A. B., "Coupled Inviscid/Viscous Aerodynamic Predictions for Supersonic Tactical Missiles," AIAA Paper 90-0617, Jan. 1990.

[18]Priolo, F. J., and Wardlaw, A. B., Jr., "Euler Space-Marching Computations with Crossflow Seperation for Missile-Type Bodies," AIAA Paper 90-0616, Jan. 1990.

[19]Wardlaw, A. B., Jr., Priolo, F. J., and Solomon, J. M., "Multiple-Zone Strategy for Supersonic Missiles," *Journal of Spacecraft and Rockets*, Vol. 24, No. 4, 1987, pp. 377–384.

[20]Wardlaw, A. B., Jr., Baltakis, F. P., Martin, F. M., Priolo, F. J., and Jettmar, R. U., "A Godunov Method for Supersonic Tactical Missiles," *Journal of Spacecraft and Rockets*, Vol. 24, No. 1, 1987, pp. 40–47.

[21]Est, B. E., and Nelson, H. F., "Aerodynamic Forces on Noncircular Cross Section Missile Forebodies," *Journal of Aircraft*, Vol. 29, No. 4, 1992, pp. 612–618.

[22]Polhamus, E. C., Geller, E. W., and Grunwald, K. J., "Pressure and Force Characteristics of Noncircular Cylinders as Affected by Reynolds Number With a Method Included for Determining the Potential Flow About Arbitrary Shapes," NASA TR R-46, March 1959.

[23]Nelson, H. F., and Talpallikar, M. V., "Fin Planform Effects on Lift and Center of Pressure for Supersonic Missiles," *Journal of Spacecraft and Rockets*, Vol. 30, No. 6, 1993, pp. 707–714.

[24]Est, B. E., and Nelson, H. F., "Fin Dihedral Effects on Aerodynamics of Supersonic Missiles with Square and Triangular Fuselage Cross Sections," *AIAA 9th Applied Aerodynamics Conference: A Collection of Technical Papers*, Vol. CP918, AIAA, Washington, DC, 1991, pp. 433–443 (AIAA Paper 91-3256).

J. E. Daywitt
Associate Editor